Environ Res Tec, Vol. 4, Issue. 4, pp. 358–368, December 2021

Environmental Research and Technology
https://ert.yildiz.edu.tr - https://dergipark.org.tr/tr/pub/ert
DOI: https://doi.org/10.35208/ert.973855

Environmental Research & Technology

Research Article

Macroporous thermoset monoliths from glycidyl methacrylate (GMA)-based high internal phase emulsions (HIPEs): Effect of cellulose nanocrystals (CNCs) as filler - Functionalization and removal of Cr(III) from aqueous solutions

Burcu KEKEVİ[*1], Ali ESLEK[2], E. Hilal MERT[3]

[1]*Department of Material and Material Processing, Yalova University, Yalova Community College, Yalova, Turkey*
[2]*Department of Polymer Materials Engineering, Yalova University, Institute of Graduate Studies, Yalova, Turkey*
[3]*Department of Polymer Materials Engineering, Yalova University Faculty of Engineering, Yalova, Turkey*

ARTICLE INFO

Article history
Received: 25 July 2021
Revised: 22 November 2021
Accepted: 25 November 2021

Key words:
Amine functionalization; Chrome (III) removal; CNC; GMA; Macroporous foam

ABSTRACT

Macroporous foams having 80 vol % of nominal porosity were synthesized by the copolymerization crosslinking of glycidyl methacrylate (GMA) based high internal phase emulsions (HIPEs). To alter the mechanical and thermal properties, cellulose nanocrystals (CNCs) were used as filler. For this purpose, CNCs were added to the continuous oil phase during emulsification process at a loading rate of 1, 5 or 7 wt %. Consequently, composite foams were obtained by purification of the polymerized HIPEs (polyHIPEs). The effect of CNCs on the morphological and mechanical properties was investigated. It was found that CNCs have a significant influence on the thermal stability and the compressive strength of the obtained foams. In the end, the neat polyHIPE foam and the polyHIPE/CNC composite foam with 1 wt % of CNC were post-functionalized by reacting phenylimidazole (PIAL) with the epoxy ring of the GMA units. Resulting amine functional foams and the neat foam were utilized in Cr(III) removal from aqueous solutions. It was demonstrated that amine functional foams have a great potential as sorbent materials. The results also showed that the existence of CNCs decreased the performance for removing Cr(III) ions. Nevertheless, functionalization by PIAL significantly improved the selectivity of Cr(III) in comperasion with the neat polyHIPE foam.

Cite this article as: Kekevi B, Eslek A, Mert EH. Macroporous thermoset monoliths from glycidyl methacrylate (GMA)-based high internal phase emulsions (HIPEs): Effect of cellulose nanocrystals (CNCs) as filler - Functionalization and removal of Cr(III) from aqueous solutions. Environ Res Tec 2021;4:4:358–368.

INTRODUCTION

Morphology is one of the main factors affecting the application area of polymeric materials. Especially for separation science and chromatography, polymeric monoliths that are exhibiting well-defined open-cellular morphology are highly preferred due to their highly permeable structure allowing mass transfer. Apart from the porous structure the

***Corresponding author.**
*E-mail address: bkekevi@yalova.edu.tr

other important parameter required for above mentioned applications is of course the chemical functionality. From this point of view a polymer monolith, in which ideal pore morphology combines with the chemical structure composed of special functional groups is the perfect material for separation and chromatography applications. To achieve this goal, since the first introduction of high internal phase emulsion (HIPE) templated polystyrene based hierarchical macroporous foams, which are known as poly(high internal phase emulsions) (polyHIPEs), by Unilever researchers Bartl and Bonnin [1], scientists are benefiting from HIPE templating for its versatility [2].

In a HIPE, the volume fraction (φ) of the internal phase (or the droplet phase) is over 0.74. This is the critical volume fraction that described by Ostwald [3, 4]. At this volume ratio the mono-disperse hard spheres are packed in the closest manner and deformed into polyhedral droplets over this value [5]. Because the adjacent droplets are separated by the thin film of continuous phase, the resulting emulsions are similar to interconnected foams. If the continuous phase is consisted of polymerizable species, polyHIPEs can be obtained [6].

Although HIPEs can be prepared as water-in-oil (w/o) or oil-in-water (o/w) emulsions depending on the continuous phase, most of the polyHIPEs are synthesized from w/o type HIPEs, which are prepared by using hydrophobic monomers [7]. In such HIPEs, the oil phase is usually composed of monomer(s), crosslinker and surfactant(s) whereas the internal phase constitutes of water. Polymerization can be achieved under mild conditions by using an oil or water-soluble initiator. Consequently, water act as a porogen and well-defined, interconnected porous structure is achieved by the removal of the porogen upon polymerization [8–10].

So far, styrene is the most common monomer used in the synthesis of polyHIPEs due to its highly hydrophobic structure [6]. Indeed, the main reason of this is preventing the coalescence of emulsion droplets and phase inversion and providing the emulsion stability. Since hydrophilic monomers tend to diffuse into the aqueous phase it is more difficult to achieve stable HIPEs by using them. However, more hydrophilic monomers such as acrylamide (AAm), 2-hydroxyl ethyl acrylate (HEA), ethylene glycol dimethacrylate (EGDMA), glycidyl methacrylate (GMA), and methyl methacrylate (MMA) have been also successfully utilized in HIPE templating [11–14]. Especially, acrylates and methacrylates have been served very well in the preparation of functional monoliths to be used as a separation and purification media, due to their chemical structure open to further functionalization reactions.

Post-polymerization functionalization is a convenient approach to gain special groups in the monolith structure. In this respect, polyGMA based monoliths offer the advantage of reactive epoxy ring. Particularly in the presence of thiols and amines, the epoxy ring can be easily opened under mild reaction conditions [15–19]. In this respect, Krajnc et al. [20] synthesized poly (GMA-ethylene glycol dimethacrylate) polyHIPE monoliths and functionalized these monoliths with different amines to investigate their capacity in the chromatographic separation of proteins. Pahovnik et al. [21] prepared hydrogel polyHIPEs through o/w type HIPEs from functionalized-polyGMA and carried out post-functionalization with different amine compounds. Consequently, they revealed the water uptake capacity of the obtained materials. In another study, Mert et al. [22] synthesized polyHIPE monoliths by the crosslinking of unsaturated polyster resin with GMA and DVB in the w/o type HIPEs. Thereafter, they carried out post-functionalization of the resulting monoliths with several amine ligands. In the end they have shown that resulting materials are highly effective in the removal of heavy metal ions. In their following study, Mert and Yıldırım also demonstrated the synthesis, functionalization and heavy metal ion uptake capacity of poly(unsaturated polyester-co-GMA-DVB) polyHIPE beads [23].

In the preparation of polyGMA based polyHIPEs, obtaining a material with high amounts of epoxy groups is challenging due to the hydrolysis of epoxy groups during polyHIPE synthesis to achieve highly functional materials [24]. However, depending on the polymerization temperature, hydrolysis amount of epoxy groups varied. Yang et al. [25] successfully utilized radiation-induced HIPE polymerization at room temperature to prepare polyGMA monoliths.

Herein, we focused on the preparation of amine functional poly(GMA-co-DVB) polyHIPE monolith and cellulose nanocrystal (CNC) loaded polyHIPE/CNC composite monoliths. For this purpose, CNC was used as filler during the preparation of polyHIPEs because it offers the advantages of biocompatibility and preparing polymers with improved properties [26–28]. Moreover, it is a cost-effective material. It is known from previous studies that the adsorption capacity of the polymers obtained by reinforcing the polymer matrix with CNC also increases significantly [27, 28]. In this respect, polyHIPE/CNC composite monoliths were obtained from the precursor HIPEs at which the amount of CNC loading was corresponding to 1, 5 or 7 wt % of the continuous oil phase. Resulting monoliths were investigated in terms of, morphological properties, thermal stability, and mechanical strength. In the end, post-polymerization functionalization reactions were also conducted by using 2-phenylimidazole (PIAL) and the capacity of the resulting functional polyHIPEs was demonstrated by utilizing in the removal of Cr(III) from aqueous solutions. In addition to all, the kinetics of the Cr(III) removal by using the resulting polyHIPE sorbents was also demonstrated. To the best of our knowledge, this is the first study describing the preparation of CNCs supported poly(GMA-co-DVB) polyHIPEs and demonstrating the synergistic influence of functionalization and CNCs loading on the removal of Cr(III) from aqueous environment.

MATERIALS AND METHODS

Materials

Glycidyl methacrylate (GMA, 97%, Sigma Aldrich), divinylbenzene (DVB, Sigma Aldrich), sorbitane monooleate (Span® 80, non-ionic surfactant, Sigma-Aldrich), poly(ethylene oxide-block-propylene oxide-block-ethylene oxide) (PEO-b-PPO-b-PEO, Mw: 4400 g/mol) (Pluronic®L-121, Aldrich), potassium persulfate (KPS, ≥99.0%, ACS reagent), Cellulose Nanocrystals (CNC) (dry powder, Dia:10–20 nm, L:300–900 nm, Nanografi), 2-Phenylimidazole (PIAL, 98%, Sigma Aldrich), dimethylformamide (DMF, 98%, Merck), calcium chloride hexahydrate ($CaCl_2.6H_2O$; 98%, Sigma-Aldrich), were used without purification. AIBN was in technical grade and used after recrystallization from ethanol. Chromium standard solution ($Cr(NO_3)_3$ in HNO_3 0.5 mol/L, 1000 mg/L Cr, CertiPUR®, Merck) was used by diluting with ultrapure deionized water.

Synthesis of polyHIPEs

GMA based polyHIPEs were prepared by 80 vol% of nominal porosity. All HIPEs were prepared by using the same experimental setup consisting of a 250 mL round bottom two-necked glass reactor equipped with an overhead stirrer and a peristaltic pump. The continuous phase was composed of GMA and DVB at a volume ratio of 9:1 and a non-ionic emulsifier mixture. The non-ionic emulsifier mixture was composed of Pluronic® L121 and Span® 80, where the volume ratio of the emulsifiers was also set to 9:1, similar as the monomer ratio in the continuous phase. In a typical experiment HIPE was prepared as described below: 40 mL of aqueous internal phase prepared by dissolving 0.4 g $CaCl_2.6H_2O$ and 1 mole % of KPS (regarding to monomers) in 40 mL of ultrapure deionized water was added to the continuous oil phase under constant stirring (@300 rpm) by droplets with the help of a peristaltic pump (pumping rate: 50 rpm). When the addition of the internal phase was completed, mixing process was continued for an additional 30 min to provide a uniform emulsion. Afterwards, precursor HIPE was transferred to sealed glass container and cured at 60 °C in an air-circulating oven for 24 h. For purification of the obtained monoliths and removal of the internal phase, monoliths were extracted by using Soxhlet apparatus in ethanol for 24 h and all samples were dried under vacuum at 40 °C after extraction.

To improve the properties of poly(GMA-co-DVB) polyHIPEs, composite monoliths was also prepared by using CNC as filler. PolyHIPE/CNC composite monoliths were also prepared by using the similar experimental procedure described above. The only difference was the addition of CNC (1 wt %, 5 wt % or 7 wt %) into the continuous oil phase before emulsification procedure. To provide homogeneous distribution of the filler continuous oil phase was homogenized at a rate of 1500 rpm for 15 min. Afterwards, the internal water phase was added as described above and the obtained HIPEs were cured. The resulting composite monoliths were names as PHC-x, where x is designating the CNC loading rate.

Post-Polymerization Functionalization of the polyHIPEs

Post-polymerization functionalization of the polyHIPEs was achieved by reacting epoxy groups of the GMA units existing on polymer chains with PIAL in mild reaction conditions. For this purpose, certain amount of polyHIPE monolith sample was cut into pieces, powdered, and placed in a 50 mL round bottom two-necked reactor equipped with a condenser. Then, 20 ml of DMF was added to swell the polyHIPE sample before the reaction. After 30 min, certain amount of PIAL corresponding to the 20% of the theoretical epoxy group content of the monolith sample was dissolved in 10 mL of DMF and added to the reactor and the temperature was increased up to 80 °C. The reaction was continued for 24 h under constant stirring at 300 rpm. In the end, functionalized polyHIPE monolith sample was filtered off and washed with DMF, ethanol and ethanol/water (1:1) mixture to remove the impurities. Then the sample was dried under vacuum at 50 °C for 48 h. The resulting functional polyHIPE monoliths were named as PHR-F and PHC-F. While PHR-F was derived from the neat polyHIPE monolith (PHR), PHC-F was derived from the polyHIPE/CNC composite monolith containing 1 wt % of CNC.

Metal Removal of Monoliths

Cr (III) metal adsorption capacity of polyHIPE/CNC composite monoliths in diluted acid solutions were determined under competitive conditions with neat polyHIPE monolith in batch experiments. For increasing adsorption capacity, 0.2 g of the neat polyHIPE monolith and polyHIPE/CNC composite monoliths were placed in aqueous Cr(III) solution. At specific time intervals, polyHIPE monoliths were filtered and the Cr(III) concentrations of the remaining solutions were investigated by Atomic Absroption Spectrometer (AAS).

Characterization

The pore morphology of the neat polyHIPE monolith and polyHIPE/CNC composite monoliths was investigated by scanning electron microscopy (SEM). For this purpose, all samples were coated by gold prior to analysis. While SEM images of the neat polyHIPE monolith was recorded by using FEI Inc., Inspect S50 model microscope, the morphology of polyHIPE/CNC composite monoliths were determined by using EDAX Philips XL-30 microscope. Average cavity size (CS) of the monoliths were calculated with the help of SEM images. In this respect, dimension of at least 50 cavities for each sample were measured from the corresponding SEM image and multiplied with a correction factor of $(2/3^{1/2})$ [29]. Then the arithmetic average and standard error were also calculated.

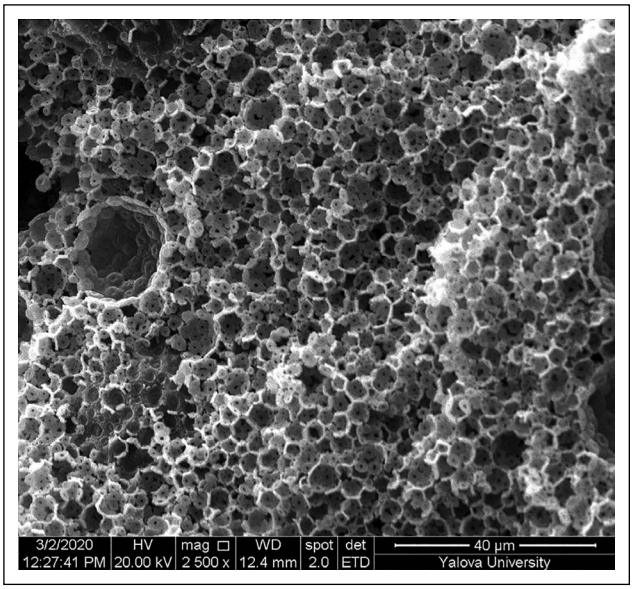

Figure 1. SEM image of the neat polyHIPE monolith (PHR).

Brunauer-Emmet-Teller (BET) specific surface area (δ_{BET}) of the polyHIPE monolith samples was measured by recording N2 adsorption/desorption isotherms on Micromeritics Gemini VII Surface Area and Porosity Analyzer. All samples were degassed flow prior to analysis under N2 and at 100 °C on Micromeritics FlowPrep 060 Sample Degas Unit. For each polyHIPE monolith sample, δ_{BET} of the 3 identical specimens were determined and the arithmetic average of the determined values was calculated as BET specific surface area (δ_{BET}).

Thermal stability of the polyHIPE monoliths was investigated by thermal gravimetrical analysis (TGA). With this aim, TGA and DTG curves were recorded between 30 °C and 650 °C by using Mettler Toledo TGA/DSC 3+ STAR system under N2 flow. During the analyses the heating rate was adjusted to 10 °C/min.

To determine the mechanical behavior of the polyHIPE monoliths under uniaxial compressive load, compression tests were performed by using a ZwickRoell Z020 Universal Testing Machine. The tests were carried out according to the testing standard (Standard Test Method for Compressive Properties of Rigid Cellular Plastics) ASTM D1621-04a. In this respect, for each polyHIPE monolith sample five different specimens with identical dimensions were prepared (15 mm height × 10 mm width). The test data were recorded on testXpert II Testing Software and the obtained data was used to draw stress vs. strain plots. The compression modulus (E_c), compressive strength (σ_L) and relative deformation at compressive strength (ε_L) were also determined by using the original software.

The chemical structure of the functional polyHIPE monoliths were confirmed by Fourier Transform Infrared Spectroscopy (FTIR) and elemental analysis. For this purpose, Perkin Elmer Spectrum 100 FT-IR spectrometer was used for FTIR analysis, while Eurovector EA3000-Single Analyser was used for elemental analysis.

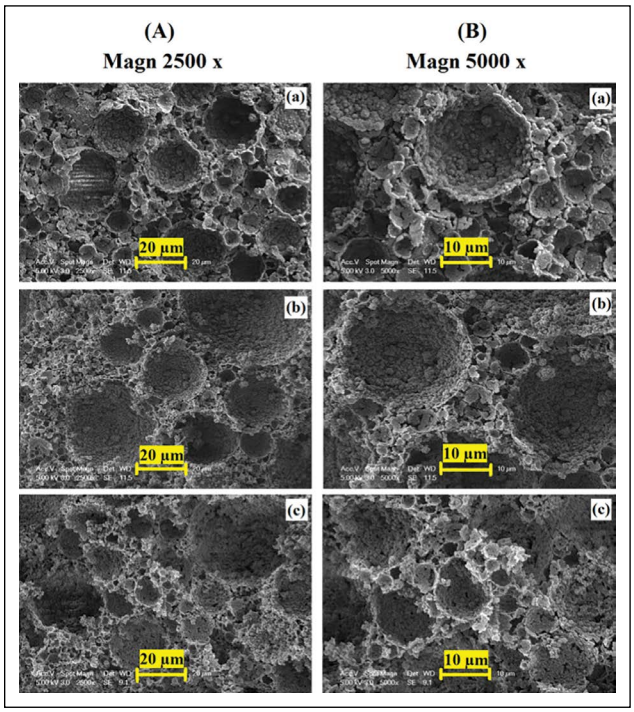

Figure 2. SEM images of the polyHIPE/CNC composite monoliths. **(a)** PHC-1, **(b)** PHC-5 and **(c)** PHC-7 at different magnification rates. (A)2500 x and (B)5000 x.

The Cr(III) removal capacity of the polyHIPE sorbents was determined by atomic absorption spectroscopy. For this purpose, Cr(III) concentrations were calculated by using the data obtained from Perkin Elmer Elmer Analyst 800 atomic absorbance spectrometer.

RESULTS AND DISCUSSION

PolyHIPE Synthesis and Characterization

To determine the influence of CNC addition on the properties of poly(GMA-co-DVB) polyHIPEs, polyHIPE/CNC composite monoliths (PHC-x) was also synthesized by varying the amount of CNC loading at a rate of 1%, 5% and 7%. In all cases, the neat polyHIPE monolith (PHR) sample and the CNC added polyHIPE/CNC composite monoliths (PHC-x) were obtained successfully by the copolymerizartion crosslinking of precursor HIPE templates. Afterwards, the influence of CNC addition on the macroporous morphology of the samples was first investigated by SEM. The SEM image of the neat polyHIPE monolith (PHR) and the polyHIPE/CNC composite monoliths (PHC-x) are presented respectively in Figure 1 and Figure 2. It was determined from Figure 1 that PHR displayed an open-cell structure with well-defined spherical pores and interconnecting pore throats pores. However, as can be seen from Figure 2, the morphology of the composite

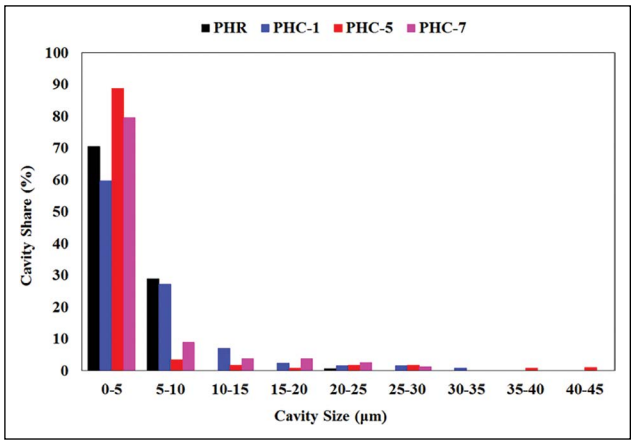

Figure 3. Cavity size distribution of the polyHIPEs.

monoliths (PHC-x) was altered by CNC loading. The most significant change that can be seen from the SEM images presented in Figure 2 that, the heterogeneous morphology, and the presence of macropores in various dimensions. Moreover, while the surface of the neat polyHIPE monoliths (PHR) was smooth, polyHIPE/CNC composite monoliths (PHC-x) were all exhibited a rough surface. In case of composite monoliths (PHC-x) the spherical pore throats were mostly replaced by the thin cracks on the surface of the macropores. This situation can be explained by the pore formation mechanism suggested by Menner and Bismarck [30]. According to their study, pore throats are originated by the rupture of the continuous polymer film formed around the internal phase droplets. The spherical geometry of the pore throats can be ascribed to the alteration of the solubility of the used emulsifier and the phase separation of the continuous phase with the progress of polymerization process. When the conversion of monomer was increased, this incident causes formation of emulsifier rich and polymer rich phases. Accordingly, emulsifier molecules that place at oil/water interface create weak points that can be rupture easily [30]. In addition, the heterogeneous morphology of polyHIPE/CNC composites is also indicating low emulsion stability, which can be associated by large cavities, possibly caused by larger droplets formed due to coalescence and Ostwald ripening [31]. In addition to all, when comparing Figure 1 and Figure 2 with the cavity size distribution graphs presented in Figure 3, it can be concluded that the increase in CNC loading increases the cavity size distribution. However, as compared to the neat polyHIPE monolith, the alteration of average cavity size of polyHIPE/CNC composite monoliths was found to be moderate (Table 1). Since the BET specific surface area (δ_{BET}) values of foams and monolithic materials is an important property for various applications, variation of BET specific surface area by the change of CNC loading rate was also investigated. According to the BET specific surface area data displayed in Table 1, it was concluded that CNC loading resulted in higher surface area.

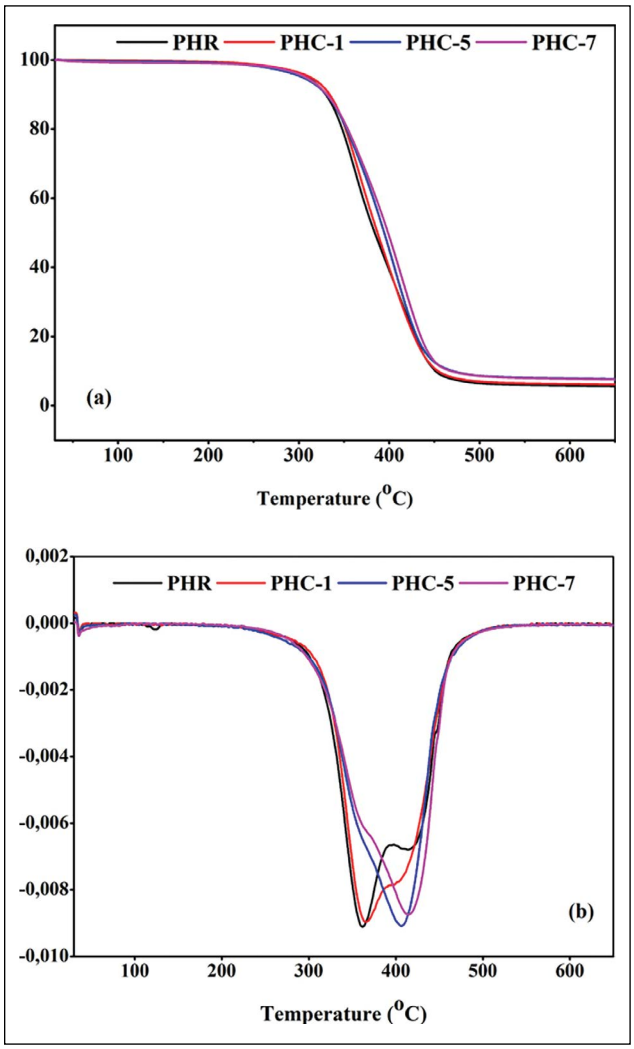

Figure 4. **(a)** TGA and **(b)** DTG thermograms of the polyHIPE monoliths.

Table 1. Average cavity size (CS) and BET specific surface area (δ_{BET}) of the polyHIPEs

Sample	CS (μm)	δ_{BET} (m^2g^{-1})
PHR	4.52	5.73
PHC-1	2.63	6.81
PHC-5	4.44	7.55
PHC-7	5.12	12.26

It is known from the earlier publications that using CNC as a filler in the polyHIPE matrix contributes to the thermal stability of the materials [26]. In this respect, the influence of CNCs on the thermal degradation behavior of the polyHIPE/CNC composite monoliths (PHC-x) was investigated against the neat polyHIPE monolith (PHR) by using TGA. The comparative TGA and DTG curves are presented in Figure 4 and the thermal data obtained from TGA is presented in Table 2.

Table 2. Thermal and mechanical properties of the polyHIPEs

Sample	Td_{10} (°C)	T_{d50}) (°C)	Residual char (wt %)	E_c (MPa)	σ_L (MPa)	ε_L (%)
PHR	324.82	378.99	5.66	15.9	0.96	5.1
PHC-1	329.28	382.17	6.12	19.3	2.46	7.6
PHC-5	325.76	389.62	7.68	21.1	2.21	5.5
PHC-7	326.17	393.79	7.58	17.2	0.57	2.8

***Td_{10}**: initial degradation temperature; **Td_{50}**: midpoint degradation temperature; **E_c**: compression modulus; **σ_L**: compressive strength **ε_L**: relative deformation at compressive strength.*

Thermal degradation of polymeric composites generally begins with the elimination of low-molecular weight compounds such as water or a monomer and continued with a larger weight loss degradation of a highly connected polymer network [32]. Depending on the TGA curves shown in Figure 4(a), it could be concluded that the degradation of the neat polyHIPE monolith (PHR) was performed in two-stage process whereas polyHIPE/CNC composite monoliths (PHC-x) were degraded in one-stage process. Particularly, the degradation steps of PHR and PHC-x monoliths could be observed from DTG curves more distinctly. In DTG curves of all monoliths, evaporation of water below 100 °C could be observed, clearly. Additionally, in the DTG curve of neat polyHIPE monolith (PHR), the weight loss detected at 140 °C arise due to the degradation of unreacted GMA monomer. The largest weight loss of PHR monolith observed in two steps that corresponded to two polymer networks crosslinked at different rates. However, the largest weight loss of polyHIPE/CNC composite monoliths performed in one step that the partial degradation transitions of polymer network had cause the DTG curve look like this. The water absorbed by hydrophilic CNC induced the degradation of the polymer network and had cause degradation at lower temperatures [33]. This partially different degradation process of PHC monoliths could be detected evidently in DTG curve of PHC-1 monolith due to strong intermolecular interactions between CNC and polymer network [34].

In Table 2, while the initial degradation temperature (Td_{10}) corresponds to the temperature at which 10% of degradation occurred, midpoint degradation temperature (Td_{50}) corresponds to the temperature at which 50% of the initial mass is degraded. As can be seen from the thermal data (Table 2), the initial degradation temperature slightly increased with the addition of CNC. On the other hand, the maximum change in initial degradation temperature was recorded for PHC-1 with an increase of ~5 °C. Although the PHC-5 and PHC-7 monoliths also exhibited higher initial decomposition temperatures as compared to the neat polyHIPE monolith (PHR), the change recorded was negligible. On the other side, the fluctuation in values was also indicating an inhomogeneous distribution of the filler.

When comparing with the neat polyHIPE monolith (PHR) the improvement of the midpoint degradation temperature of the polyHIPE/CNC composite monoliths (PHC-x) was more obvious. It was found that the increase in the midpoint degradation was reached to 14.8 oC for the composite monolith containing 7 wt % of CNC. In addition to all, the residual char determined by TGA is given in Table 2. It can be seen from Table 2 that due to the addition of CNC the residual char recorded for the polyHIPE/CNC composite monoliths (PHC-x) was also increased, as compared to the neat polyHIPE monolith (PHR).

To determine the influence of CNC addition on the mechanical properties, compressive features of the neat polyHIPE monolith (PHR) and polyHIPE/CNC composite monoliths (PHC-x) were investigated. Compressive stress vs. strain plots of the samples is presented in Figure 5, while the data obtained by the tests are given in Table 2. As can be seen from Figure 5 and Table 2, CNC addition has a great influence on the variation of mechanical properties, namely compression modulus (E_c), compressive strength (σ_L) and relative deformation at compressive strength (ε_L). When comparing with the mechanical data of the neat polyHIPE (PHR) sample, it was determined that the compression modulus and compressive strength were first increased and then decreased at the highest loading ratio of CNC. It was also found that the relative deformation of the polyHIPE/CNC composite monoliths (PHC-x) was first slightly increased at a loading ratio of 1 wt % and then decreases significantly when the CNC loading ratio was corresponding to 7 wt %.

Functionalization of polyHIPEs

To demonstrate a possible field of application and to obtain polyHIPE sorbents, post-polymerization functionalization was carried out. In this respect, the polyHIPE/CNC composite synthesized by using 1 wt % of CNC (PHC-1) was selected considering both morphological, thermal, and mechanical properties. The neat polyHIPE monolith (PHR) was also used for the same purpose as a reference material. Functionalization was achieved over the epoxy ring of GMA units using PIAL. The achievement of functionaliza-

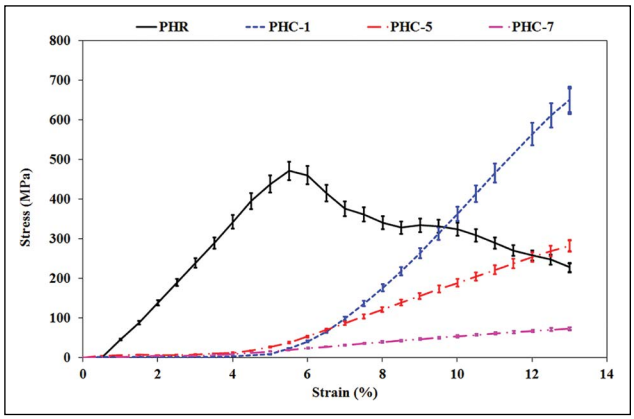

Figure 5. Compressive stress vs. strain plots of the polyHIPEs.

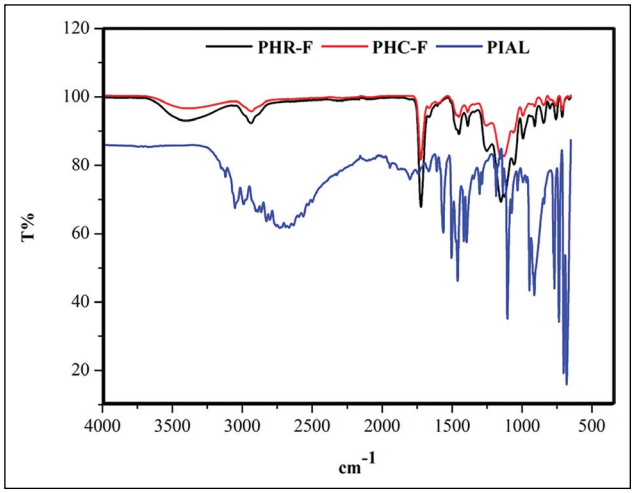

Figure 6. Comparative FTIR spectra of the functionalized polyHIPEs (PHR-F and PHC-F) and PIAL.

Table 3. Elemental analysis data and the calculated degree of functionalization of the functionalized polyHIPEs (PHR-F and PHC-F).

Sample	Theoretical	Experimental	Functionalization degree (%)
	N %	N %	
PHR-F	2.76	1,227	44.46
PHC-F	2.76	1,399	50.68

tion was confirmed via FTIR and comparative FTIR spectra of the functional monoliths (PHR-F and PHC-F) and PIAL are presented in Figure 6.

In the FTIR spectra of PHR-F and PHC-F presented in Figure 6, the characteristic peaks at 1726 cm^{-1} and in the range between 1200 cm^{-1} – 1100 cm^{-1} corresponds to the ester bonds. Moreover, the band between 1600 cm^{-1} –1450 cm^{-1} and the peak at 709 cm^{-1} is corresponding to the aromatic ring and these absorption peaks are appeared in the spectra of both functionalized polyHIPEs (PHR-F and PHC-F) and

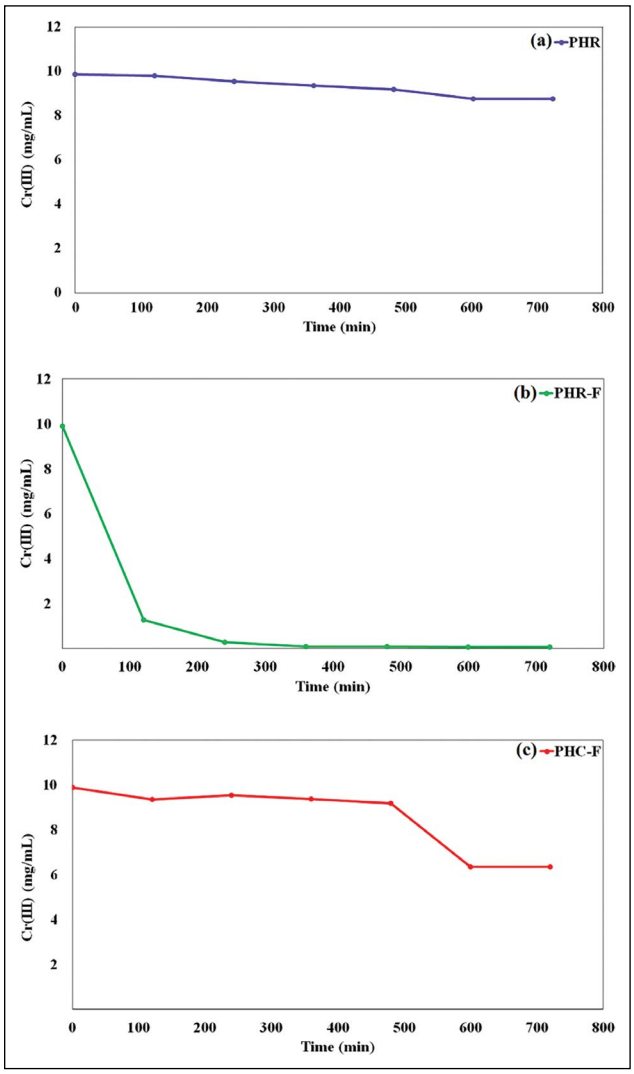

Figure 7. Kinetics of Cr(III) removal with polyHIPEs: **(a)** the neat polyHIPE (PHR), **(b)** functionalized neat polyHIPE (PHR-F), **(c)** functionalized polyHIPE/CNC (PHC-F).

the PIAL. Finally, the band between 1440 cm^{-1} – 1480 cm^{-1} and the peak appeared at 2930 cm^{-1} are due to the aliphatic groups. Since new bonds are formed with the reaction of PIAL with epoxy ring, the absorption peak corresponding to the epoxy ring (907 cm^{-1}) in the spectra of functionalized polyHIPEs (PHR-F and PHC-F) was expected to be decreased or completely disappeared. In this respect, it can be seen from Figure 6 that, the signals of the peak expected to be appeared at 908 cm^{-1} decreased distinctly and shifted to a lower area (at 899 cm^{-1}), as expected. In addition to this, the band observed in the spectra of functional polyHIPEs (PHR-F and PHC-F) at 1400 cm^{-1} can be attributed to the C-N bonds. In the spectra of PHC-F, the broad peak observed at 3450 cm^{-1} corresponds to the –OH groups of CNCs. On the other hand, the C-O stretching band of CNCs was overlapped with C-O stretching of GMA units and appeared as an intense, necked peak at 1262 cm^{-1}.

Table 4. The kinetic data and R-square (R2) values of the plots

		PHR	PHR-F	PHC-F
Pseudo-first order kinetic model	Q_e (mg/g)	0.0318	0.0107	0.0339
	k'_1 (L/min)	1.8424×10^{-4}	0.8521×10^{-4}	6.9090×10^{-4}
	R^2	0.9630	0.8758	0.7104
Pseudo-second order kinetic model	Q_e (mg/g)	-	1.9044	1.2770
	k'_2 (L/min)	-	0.0681	3.6010×10^{-4}
	R^2	0.0019	0.9995	0.0173

In order to determine the degree of functionalization, the N % quantity of the functionalized polyHIPEs (PHR-F and PHC-F) was determined by elemental analysis and used together with the theoretical N % quantity to calculate the degree of functionalization. The theoretical and experimental N % values and calculated degree of functionalization are demonstrated in Table 3. It can be seen from Table 3 that the degree of functionalization was performed with a yield of 50.68% for PHC-F and 44.46% for PHR-F.

Cr(III) Removal by polyHIPEs

The applicability of the resulting poly GMA based neat polyHIPE (PHR), functionalized neat polyHIPE (PHR-F) and polyHIPE/CNC composite (PHC-F) as polymeric sorbent materials was investigated in the removal of Cr(III) from aqueous solutions, under non-competitive conditions. It can be seen from Figure 7 that the amount of the removed Cr(III) was increased with the increase of contact time. However, the kinetic curves presented reveals the influence of the structure of sorbent matrix used for Cr(III) removal. According to Figure 7, both functionalized monoliths (PHR-F and PHC-F) exhibited higher efficiency in the removal of Cr(III) as compared to the neat polyHIPE (PHR). In case of PHR, the process occurred relatively slow and the equilibrium has been reached after 500 min As well as the equilibrium has also been reached after 500 min when PHC-F was used, this sorbent was found to be more efficient in Cr(III) removal with regards to the neat polyHIPE (PHR). On the other hand, PHR-F sorbent was found to exhibit high sorption rate and equilibrium reached after 300 min. As can be also seen from Figure 8, which demonstrates the removal efficiency of Cr(III) due to the type of polyHIPE sorbent, the percentage of the removed Cr(III) was reached as high as 98% in the case while PHR-F was used as sorbent. Since the PHR-F was obtained by post-polymerization functionalization of the neat polyHIPE monolith (PHR), these two sorbent materials basically have the same polymer skeleton. However, PHR only showed 12.5% of removal efficiency against Cr(III). Therefore, this result can be attributed to the contribution of the functional groups of PHR-F sorbent. On the other hand, it was found by

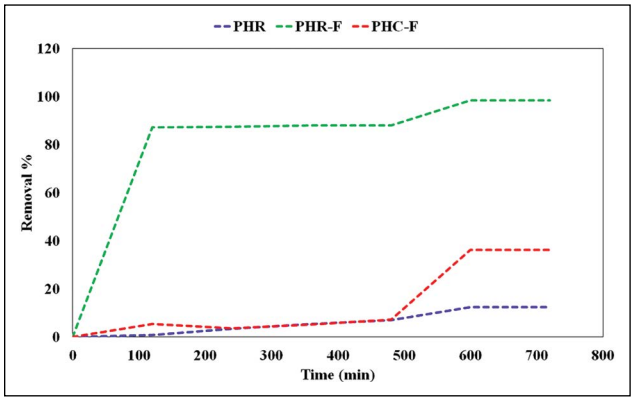

Figure 8. The removal efficiency of Cr(III) with polyHIPEs.

comparing the removal efficiency of two functionalized polyHIPE sorbents (PHR-F and PHC-F), that the PHC-F showed almost 60% lower removal efficiency. This significantly lower removal efficiency can be explained by the pore morphology of the resulting materials. As can be seen from the SEM images of the neat polyHIPE monolith (PHR) and the polyHIPE/CNC composite monolith containing 1 wt % of CNCs (PHC-1) (Figure 1 and Figure 2(a), respectively), the neat polyHIPE monolith has a more open pore structure. We believe that the more open sorbent matrix allows the diffusion of Cr(III) more easily, which probably resulted in higher removal efficiency. Since this situation also strengthens access to functional groups, this sorbent may also have shown lower activity, although it has a higher degree of functionality.

Adsorption Kinetics

To describe the kinetic process, the experimentally obtained kinetic data was fitted into Lagergren pseudo first-order and Ho's pseudo second-order kinetic model by using the linearized rate equations given in equations (1) and (2), respectively [35].

$$\ln (Q_e - Q_t) = \ln Q_e - k'_1 t \quad (1)$$

$$t/Q_t = 1/ (k'_2 Q_e^2) + t/Q^e \quad (2)$$

where Q_e (mg/g) and Q_t (mg/g) are the absorption capacities at equilibrium and time t (min), respectively. k'_1 is the pseudo-first order and k'_2 is the pseudo-second order rate constants. To calculate the Q_e and kinetic rate constants

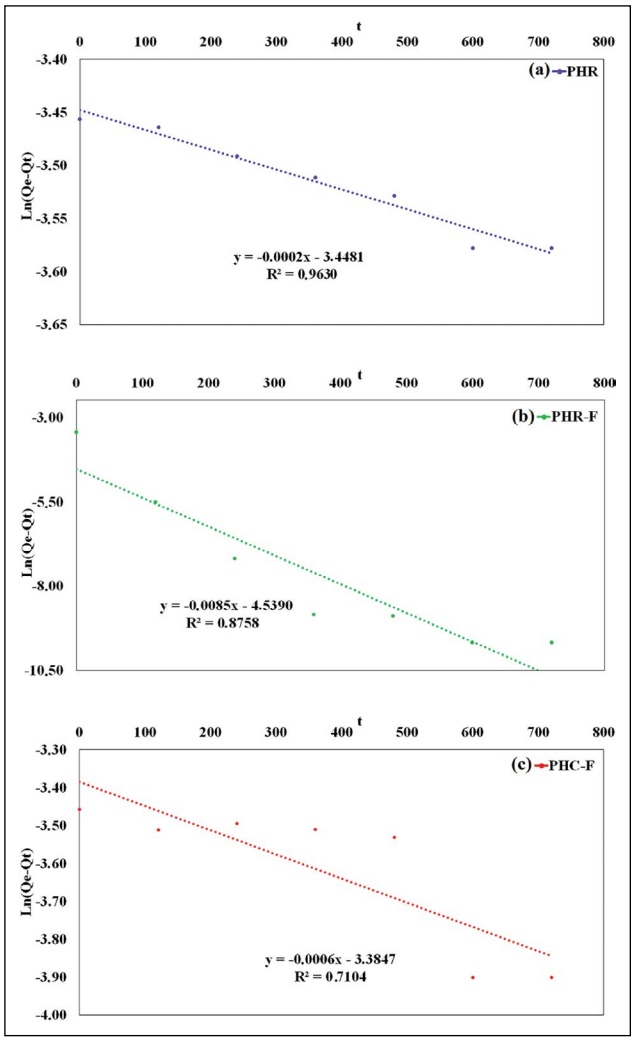

Figure 9. The kinetic plots of Cr(III) removal by polyHIPEs based on pseudo-first order kinetic model: **(a)** the neat polyHIPE (PHR), **(b)** functionalized neat polyHIPE (PHR-F), **(c)** functionalized polyHIPE/CNC (PHC-F).

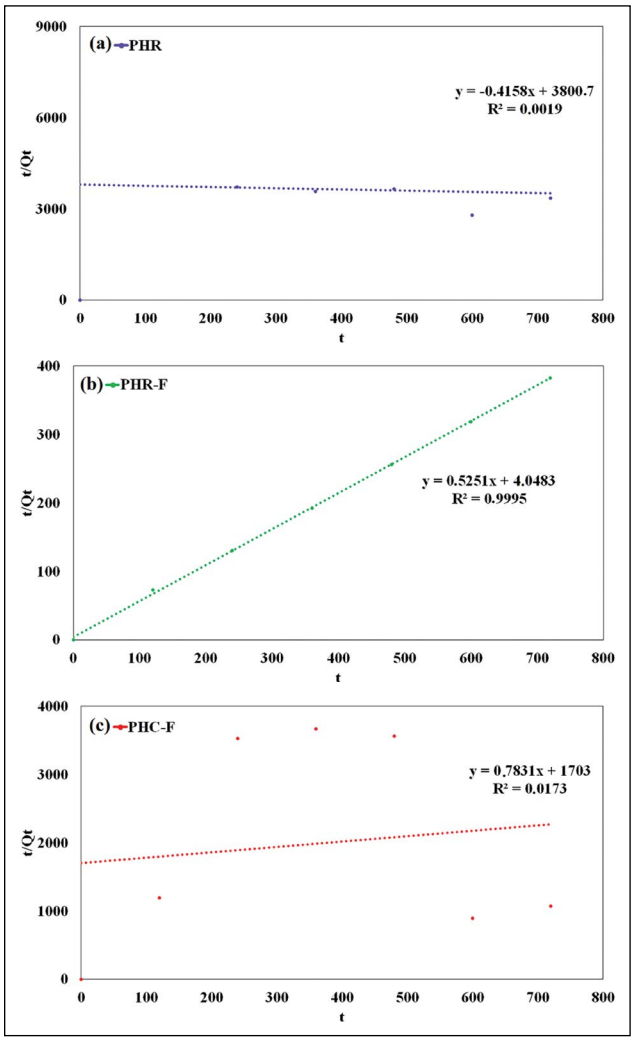

Figure 10. The kinetic plots of Cr(III) removal by polyHIPEs based on pseudo second-order kinetic model: **(a)** the neat polyHIPE (PHR), **(b)** functionalized neat polyHIPE (PHR-F), **(c)** functionalized polyHIPE/CNC (PHC-F).

experimental data were plotted according to equations (1) and (2). The obtained plots are presented in Figure 9 and Figure 10. Afterwards, kinetic rate constants and Q_e values were calculated from the slope of the linear plots and the points where the graphs cut the y-axis. The calculated kinetic data and R-square (R^2) values of the plots are given in Table 4. Since the Lagergren pseudo–first-order model is relied on the assumption that the rate of change of adsorption by time is proportional to the change in saturation concentration and the amount of adsorption by time, it is generally applicable over the initial stage of an adsorption process [36] (Sahoo and Prelot, 2020). The initial first few minutes of adsorption is usually faster, this then changes to a slower rate which is maintained as equilibrium is approached. The two different rates (chemically-controlled rate determining step or diffusion-controlled rate determining step) suggest the presence of two different adsorption sites (readily accessible external and macropore sites, and less accessible meso- and micropore sites) [37] (Li et.al, 1999). It is usually observed that when the adsorption occurs via diffusion through the interface, the kinetics of the process follows Lagergren pseudo–first-order rate equation. In this study, polyHIPEs sorbents are exhibiting similar macroporous morphology. The differences between the R^2 values can be attributed to the presence of CNC and the functional groups. The low R^2 values obtained for PHC-F, might be a reason of low affinity of PHC-F to Cr(III). This can be attributed to the fact that the interactions between the ligand molecule and the CNC are stronger than their interactions with Cr(III), and the diffusion rate might be decreased. The high R^2 values of the graph can be considered as an indication that the polyHIPE sorbents follow the kinetic model expressed by the mathematical equa-

tion used to plot the experimental data. In this respect, it can be safely stated that sorption of Cr(III) on to the neat polyHIPE (PHR) followed pseudo first-order kinetic model, while the sorption on to the functionalized neat polyHIPE (PHP-F) followed pseudo second-order kinetic model. Moreover, in the case of functionalized polyHIPE/CNC composite (PHC-F) sorbent, the pseudo-first-order kinetic model correlated relatively well with the experimental data, with a relatively low R^2 value (0.7104).

CONCLUSION

As a conclusion, to prepare polyHIPE materials exhibiting the potential of post-polymerization functionalization precursor HIPEs composed of GMA and DVB were used as templates. Moreover, CNC was also used as filler during the preparation of the precursor HIPEs for tuning the morphological, mechanical, and thermal properties of the corresponding polyHIPE monoliths. It was shown that CNC has a significant influence on morphological and mechanical properties, as well as thermal stability. In addition, post-polymerization functionalization with PIAL was performed to prepare functional monoliths using the epoxy ring on the polymer chains. It was confirmed that the degree of functionalization was 44.46% for the neat polyHIPE monolith and 50.68% for the polyHIPE/CNC composite. Based on these results, functionalized polyHIPEs and the neat polyHIPE were used for Cr(III) removal from aqueous solutions under non-competitive conditions. It was demonstrated that the Cr(III) removal capacity of the polyHIPEs was significantly improved by post-polymerization functionalization. Moreover, it was also shown that the Cr(III) removal capacity strongly depends on the pore morphology of the polyHIPE sorbents. When the removal efficiency of the neat polyHIPE was only 12.5%, the capacity of Cr(III) removal of the functionalized polyHIPE and polyHIPE/CNC composite was respectively found to be 98% and 36%.

DATA AVAILABILITY STATEMENT

The authors confirm that the data that supports the findings of this study are available within the article. Raw data that support the finding of this study are available from the corresponding author, upon reasonable request.

CONFLICT OF INTEREST

The authors declared no potential conflicts of interest with respect to the research, authorship, and/or publication of this article.

ETHICS

There are no ethical issues with the publication of this manuscript.

REFERENCES

[1]. H. Bartl and W. Bonnin, "Über die polymerisation in umgekehrter emulsion," Die Makromolekulare Chemie, Vol. 57, pp.74–95, 1962. (Deutsch)

[2]. K.M.L. Taylor-Pashow and J.G. Pribyl, "PolyHIPEs for Separations and Chemical Transformations: A Review," Solvent Extraction and Ion Exchange, Vol. 37, pp. 1–26, 2019.

[3]. N.R. Cameron and D.C. Sherrington, "High internal phase emulsions (HIPEs) — Structure, prop-erties and use in polymer preparation," Biopolymers Liquid Crystalline Polymers Phase, Emulsion. Advances in Polymer Science, Vol. 126, pp. 163–214, 1996.

[4]. W. Ostwald, "Beiträge zur kenntnis der emulsionen," Colloid and Polymer Science, Vol. 6, pp.103–109, 1910. (Deutsch)

[5]. K.J. Lissant, "The geometry of high-internal-phase-ratio emulsions," Journal of Colloid and Interface Science, Vol. 22, pp. 462–468, 1966.

[6]. H.H. Mert, M.S. Mert and E.H. Mert, "A statistical approach for tailoring the morphological and mechanical properties of polystyrene PolyHIPEs: looking through experimental design," Materials Research Express, Vol. 6, Article 115306, 2019.

[7]. S.D. Kimmins and N.R. Cameron, "Functional porous polymers by emulsion templating: recent advances," Advanced Functional Materials, Vol. 21, pp. 211–225, 2011.

[8]. S. Yang, L. Zeng, Z. Li, X. Zhang, H. Liu, C. Nie and H. Liu, "Facile approach to glycidyl methacrylate-based polyHIPE monoliths with high epoxy-group content," European Polymer Journal, Vol. 57, 127–136, 2014.

[9]. N. Brun, S. Ungureanu, H. Deleuze and R. Backov, "Hybrid foams, colloids and beyond: From design to applications," Chemical Society Reviews, Vol. 40, pp. 771–788, 2011.

[10]. M. S. Silverstein, "Emulsion-templated porous polymers: a retrospective perspective," Polymer, Vol. 55, pp. 304–320, 2014.

[11]. J. M. Williams, A. J. Gray, and M. H. Wilkerson, "Emulsion stability and rigid foams from styrene or divinylbenzene water-in-oil emulsions," Langmuir, Vol. 6, pp. 437–444, 1990.

[12]. R. Butler, I. Hopkinson, and A. I. Cooper, "Synthesis of porous emulsion-templated polymers using high internal phase CO2-in-water emulsions," Journal of American Chemical Society, Vol.125, pp. 14473–14481, 2003.

[13]. C.H. Yao, L. Qi, H.Y. Jia, P.Y. Xin, G.L. Yang, and Y. Chen, "A novel glycidyl methacrylate-based monolith with sub-micron skeletons and well-defined macropores," Journal of Material Chemistry, Vol. 19, pp. 767–772, 2009.

[14]. P.M. Solozhenkin and A.I. Zouboulis, "Removal of arsenic compounds by chemisorption filtration,"

Journal of Mining Science, Vol.43, pp. 212–220, 2007.

[15]. S. De and A. Khan, "Efficient synthesis of multifunctional polymers via thiol–epoxy "click" chemistry," Chemical Communications, Vol. 48, pp. 3130–3132, 2012.

[16]. A. Brändle, A. Khan, Thiol–epoxy 'click' polymerization: efficient construction of reactive and functional polymers," Polymer Chemistry, Vol. 3, pp. 3224–3227, 2012.

[17]. I. Gadwal and A. Khan, "Protecting-group-free synthesis of chain-end multifunctional polymers by combining ATRP with thiol–epoxy 'click' chemistry," Polymer Chemistry, Vol. 4, pp. 2440–2444, 2013.

[18]. H. Gao, M. Elsabahy, E. V. Giger, D. Li, R. E. Prud'homme, and J.-C. Leroux, "Aminated linear and star-shape poly(glycerol methacrylate)s: synthesis and self-assembling properties," Biomacromolecules, Vol. 11, pp. 889–895, 2010.

[19]. F. J. Xu, M. Y. Chai, W. B. Li, Y. Ping, G. P. Tang, W. T. Yang, J. Ma and F. S. Liu, "Well-defined poly(2-hydroxyl-3-(2-hydroxyethylamino)propyl methacrylate) vectors with low toxicity and high gene transfection efficiency," biomacromolecules, Vol.11, pp. 1437–1442, 2010.

[20]. P. Krajnc, N. Leber, D. Štefanec, S. Kontrec, and A. Podgornik, "Preparation and characterisation of poly(high internal phase emulsion) methacrylate monoliths and their application as separation media," Journal of Chromatography A, Vol. 1065, pp. 69–73, 2005.

[21]. D. Pahnovik, J. Majer, E. Zagar, S. Kovacic, "Synthesris of hydrogel polyHIPEs from functionalized glycidyl methacrylate," Polymer Chemistry, Vol. 7, pp. 5132–5138, 2016.

[22]. E. H. Mert, M. A., Kaya, and H. Yıldırım, "Preparation and characterization of polyester–glycidyl methacrylate polyHIPE monoliths to use in heavy metal removal: Functional polyHIPE monoliths as metal sorbent," Designed Monomers and Polymers, Vol. 15, pp. 113–126, 2012.

[23]. E. H. Mert and H. Yıldırım, "Porous functional poly(unsaturated polyester-co-glycidyl methacrylate-co-divinylbenzene) polyHIPE beads through w/o/w multiple emulsions: preparation, characterization and application", E-Polymers, Vol. 14, pp. 65–73, 2014.

[24]. S. Yang, L. Zeng, Y. Wang, X. Sun, P. Sun, H. Liu, C. Nie, and H. Liu, "Facile approach to glycidyl methacrylate-based polyHIPE monoliths with high epoxy-group content," Colloid and Polymer Science, Vol. 292, 2563–2570, 2014.

[25]. S. Yang, Y. Wang, Y. Jia, X. Sun, P. Sun, Y. Qin, R. Li, H. Liu, and C. Nie, "Tailoring the morphology and epoxy group content of glycidylmethacrylate-based polyHIPE monoliths via radiation-inducedpolymerization at room temperature," Colloid and Polymer Science, Vol. 296, pp. 1005–1016, 2018.

[26]. H.H. Mert, M.R. Moghbeli, S. Sajad and E.H. Mert, "Functionalized cellulose nanocrytals (fCNCs) reinforced PolyHIPEs: Tailoring morphological, mechanical and thermal properties," Reactive and Functional Polymers, Vol. 151, 104572, 2020.

[27]. L. Jin, Q. Sun, Q. Xu, and Y. Xu, "Adsorptive removal of anionic dyes from aqueous solutions using microgel based on nanocellulose and polyvinylamine," Bioresource Technology, Vol. 197, pp. 348-355, 2015.

[28]. H. Qiao, Y. Zhou, F. Yu, E. Wang, Y. Min, Q. Huang, L. Pang and T. Ma, "Effective removal of cationic dyes using carboxylate-functionalized cellulose nanocrystals," Chemosphere, Vol. 141, pp. 297-303, 2015.

[29]. A. Barbetta and N.R. Cameron, "Morphology and surface area of emulsion-derived (polyHIPE) solid foams prepared with oil-phase soluble porogenic solvents: span 80 as surfactant," Macromolecules, Vol. 37, pp. 3188–3201, 2004.

[30]. A. Menner and A. Bismarck, "New evidence for the mechanism of the pore formation in polymerising high internal phase emulsions or why polyHIPEs have an interconnected pore network structure," Macromolecular Symposia, Vol. 242, pp. 19–24, 2006.

[31]. R.J. Carnachan, M. Bokhari, S.A. Przyborskibc and N.R. Cameron, "Tailoring the morphology of emulsion-templated porous polymers," Soft Matter, Vol. 2, pp. 608–616, 2006.

[32]. E. Lizundia, J.L.Vilas and L.M. León, "Crystallization, structural relaxation and thermal degradation in Poly (L-lactide)/cellulose nanocrystal renewable nanocomposites," Carbohydrate Polymers, Vol. 123, pp. 256–265, 2015.

[33]. F.J. Kilzer and A. Broido, "Speculations on the nature of cellulose pyrolysis," Pyrodynamics, Vol. 2, pp. 151–163, 1965.

[34]. S. Maiti, J. Jayaramudu, K. Das, S.M. Reddy, R. Sadiku, S.S. Ray and D. Liu, "Preparation and characterization of nano-cellulose with new shape from different precursor," Carbohydrate Polymers, Vol. 98, pp. 562–567, 2013.

[35]. R. Elangovan, L. Philip and K. Chandraraj, "Biosorption of chromium species by aquatic weeds: Kinetics and mechanism studies," Journal of Hazardous Materials, Vol. 152, pp. 100–112, 2008.

[36]. T.R. Sahoo, B. Prelot, "Nanomaterials for the detection and removal of wastewater pollutants," Micro and Nano Technologie, pp. 161–222, 2020.

[37]. P.H.Y. Li, R.L. Bruce, M.D. Hobday, "A pseudo first order rate model for the adsorption of an organic adsorbate in aqueous solution," Journal of Chemical Technology and Biotechnology, Vol. 74, pp. 55-59, 1999.